Design of 980 nm-Pumped Waveguide Laser for Continuous Wave Operation in Ion Implanted Er:$LiNbO_3$

Sohel Mahmud Sher, Paolo Pintus, *Student Member, IEEE*, Fabrizio Di Pasquale, *Member, IEEE*, Marco Bianconi, Giovanni Battista Montanari, Pietro De Nicola, Simone Sugliani, and Giancarlo Prati, *Fellow, IEEE*

***Abstract*— Embedded channel waveguides formed on a *z*-cut erbium-doped lithium niobate (Er:$LiNbO_3$) substrate by a high-energy ion implantation technique are first described. A detailed theoretical design of a waveguide laser for continuous wave operation is then discussed, taking into account realistic input parameters and measured data. To simulate waveguide modes and to predict laser outputs from our fabricated waveguide sample, a numerical tool is developed in FORTRAN based on the full vectorial finite element method. Using the developed tools, the waveguide dimension is optimized, ensuring single-mode operation at both pump (980 nm) and laser (1531 nm) wavelengths. Finally, laser outputs as a function of various waveguide parameters are analyzed. The proposed analysis allows the effective optimization of the ion-implanted waveguide laser in Er:$LiNbO_3$.**

***Index Terms*— Embedded channel waveguide, erbium, ion implantation, lithium niobate, waveguide laser design.**

I. Introduction

ERBIUM-DOPED lithium niobate (Er:$LiNbO_3$) waveguide lasers operating in the third telecommunication window ($\sim$1.55 μm wavelengths) have attracted attention in the last few years. In lithium niobate higher erbium concentrations are achievable without ion clustering due to the fact that erbium ions occupy regular positions in the crystal lattice [1]. The combination of amplifying properties of erbium ions with the excellent electro-optical properties of lithium niobate allows the development of several interesting waveguide devices with higher functionality [2]. Among the several methods of waveguide fabrication in $LiNbO_3$, ion implantation is attractive because it allows precise control of waveguide geometry and low degradation of electro-optical properties [3].

Manuscript received June 25, 2010; revised September 22, 2010; accepted November 1, 2010. Date of current version March 16, 2011. This work was supported in part by the Ministry of University and Research, Italy, under Project prot.2007N43PRT.

S. M. Sher, P. Pintus, F. Di Pasquale, and G. Prati are with the Scuola Superiore Sant'Anna, Centre of Excellence for Information, Communication and Perception Engineering, Pisa 56124, Italy (e-mail: m.sohel@sssup.it; p.pintus@sssup.it; f.dipasquale@sssup.it; giancarlo.prati@cnit.it).

M. Bianconi, G. B. Montanari, P. De Nicola, and S. Sugliani are with the Institute for Microelectronics and Microsystems of the National Research Council, Bologna 40129, Italy (e-mail: bianconi@bo.imm.cnr.it; montanari@bo.imm.cnr.it; denicola@bo.imm.cnr.it; sugliani@bo.imm.cnr.it).

Color versions of one or more of the figures in this paper are available online at http://ieeexplore.ieee.org.

Digital Object Identifier 10.1109/JQE.2010.2094603

So far, $LiNbO_3$ waveguides formed by the implantation of various ions, including H, He, B, C, N, O, F, Si, P, Ti, Cu, Ni and Ag, with different electrovalence, energies and fluences have been studied [4]. Previous studies focus mainly on the fabrication and refractive index characterization of $LiNbO_3$ waveguides by implantation of ions at both low and high doses. Recently, ion implantation has also shown its effectiveness for developing novel $LiNbO_3$ thin film through the ion slicing and wafer bonding technique, producing microring resonators of submicron radii with low bending losses [5]–[7]. First realization of photonic crystal structures in such thin films has also been reported [8]. Moreover ion implantation allows the fabrication of ridge waveguides with very low roughness [9].

In this paper, we present a steady state model of a z-cut y-propagating Er:$LiNbO_3$ waveguide laser fabricated by high energy carbon (C^{3+}) ion implantation. The refractive index variation along the waveguide depth caused by the ion implantation process includes both enhanced (for extraordinary index) and barrier-like (for ordinary index) profiles that are measured and characterized experimentally. When forming optical waveguides by ion implantation, the resulting refractive index profiles after annealing must be experimentally characterized and fully understood for design optimization. Modal analysis in these waveguides is rather difficult and requires powerful numerical techniques. For this purpose, waveguide modes and steady state laser operations are fully described in our model which combines a full vectorial finite element method (VFEM) and a Runge-Kutta (RK) algorithm [10].

The computational tool we developed allows us to consider the strong anisotropy of $LiNbO_3$ crystal along with the arbitrary index behaviour of the implanted waveguide. Our numerical model predicts efficient lasing action at 1531 nm from the fabricated waveguide sample. Laser outputs are analyzed as a function of coupled pump power, cavity length, output mirror reflectivity, excited state absorption and background losses. Such analysis allows us to optimize the design of ion implanted waveguide lasers in order to achieve high efficiency. Although our model focuses mainly on an ion-implanted waveguide, it can be used for waveguides fabricated by other methods as well.

This paper is organized as follows. Section II briefly describes the technology used for fabricating ion implanted embedded channel waveguides in Er:$LiNbO_3$. In section III,

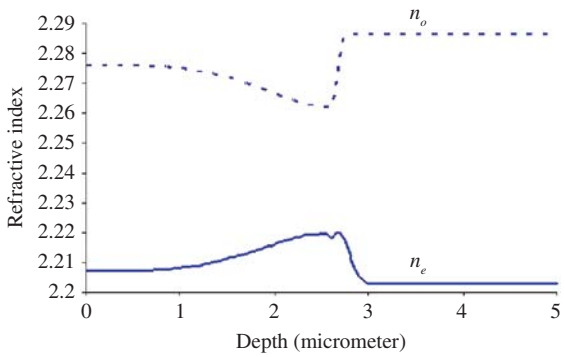

Fig. 1. Ordinary (n_o) and extraordinary (n_e) index profiles at 632.8 nm of $LiNbO_3$ (assumed equal to Er:$LiNbO_3$, see text for details) after implantation of C^{3+} ions at energy of 3.9 MeV and a fluence of 1.65×10^{15} ions/cm^2 with 2 hours annealing at 270 °C in oxygen.

a finite element method based modal analysis is presented for z-cut ion implanted Er:$LiNbO_3$ waveguides in order to compute optical modes at both laser (1531 nm) and pump (980 nm) wavelengths. A formulation of the steady state laser model is outlined in section IV. The laser design for continuous wave (CW) operations is discussed in section V. In Section VI, we discuss the laser performance and investigate the impacts of different waveguide parameters. Section VII provides a summary as well as some concluding remarks.

II. Waveguide Formation by Ion Implantation

The comparison between dark m-lines measurements of slab waveguides obtained on undoped ($LiNbO_3$) and doped (Er:$LiNbO_3$) material, reported respectively in [11] and [12], allows us to assume, as a reasonable approximation, that the refractive index profiles for both cases are equal under the same ion implantation conditions. Therefore the index profiles were engineered to be suitable for WDM applications following the procedure proposed in [11] for the undoped material.

Planar optical waveguides were fabricated in order to confirm the predicted profiles. Implantation of carbon (C^{3+}) ions was performed, using the 1.7 MV tandem accelerator at the CNR-IMM Institute of Bologna, on a z-cut $LiNbO_3$ sample at the energy of 3.9 MeV and a dose of 1.65×10^{15} ions/cm^2. In order to avoid channelling effects, the samples were tilted 7° around the X-axis and then 22° around the Z-axis. After the implantation, the samples were annealed at 270°C for 2 hours in oxygen atmosphere.

The damage induced in the crystal after this process is mainly due to nuclear collisions (nuclear damage regime) which are more effective near the ions end of range (2.6 μm below the surface). The resulting refractive index profiles shown in Fig. 1 are consistent with both the m-lines spectroscopy measurements and the profiles predicted on the basis of the model reported in [11].

The ordinary index profile (n_o) shows the typical barrier-like shape whereas the extraordinary index profile (n_e) shows a buried-raised index shape. This behaviour can generically be ascribed to a reduction of $LiNbO_3$ anisotropy (decrease in n_o, increase in n_e) induced by the local breaking of the crystal order.

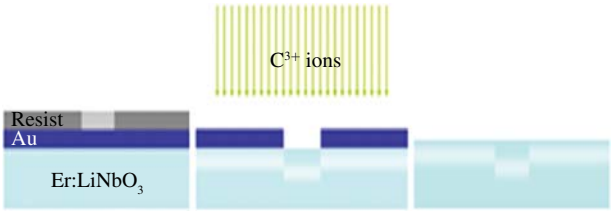

Fig. 2. Schematic of the fabrication of embedded waveguide by ion implantation in Er:$LiNbO_3$ substrate.

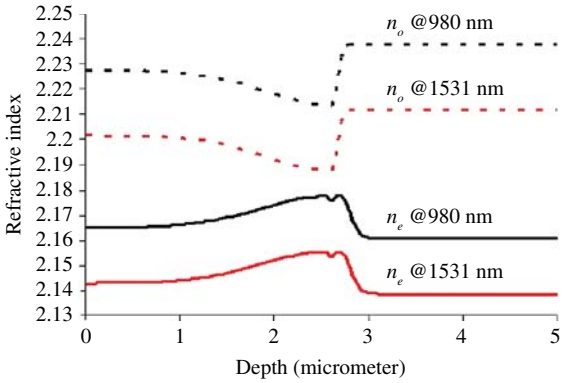

Fig. 3. Ordinary (n_o) and extraordinary (n_e) refractive index profiles at pump (980 nm) and signal (1531 nm) wavelengths for ion implanted $LiNbO_3$ (assumed equal to Er:$LiNbO_3$ see text for details) achieved by interpolating the measured data (at 632.8nm) of Fig. 1 through Sellmeier fitting.

In the next section we will present a modelling of the embedded waveguide routinely fabricated in our labs. The process includes a wet-etching definition of the 1.1 μm thick gold (Au) layer previously evaporated on the z-cut Er:$LiNbO_3$ surface and masked with a photoresist. After subsequent etching and removal of the photoresist, carbon ions are implanted on the sample surface (see Fig. 2). The damaged layer under the mask-covered area lies just beneath the surface sample because of the stopping effect of the Au mask on impinging C^{3+} ions. The damage is extended to a longer range under the uncovered portion of the sample (waveguide core). Thus, an index contrast is also created in the horizontal direction, providing a lateral confinement of optical power.

III. Finite Element Method Based Modal Analysis

From Fig. 1, we observe that the measured ordinary index profile has a typical barrier shape whereas the extraordinary one is characterized by a buried-raised index profile.

In order to perform a modal analysis of the waveguide at both laser and pump wavelengths, we first draw (see Fig. 3) the profiles at both 980 nm and 1531 nm by a numerical fit based on the Sellmeier equation of the $LiNbO_3$ crystal [13]. Note that Fig. 3 presents both the ordinary and extraordinary profiles at the wavelengths under consideration. We consider the same Sellmeier equation for both Er:$LiNbO_3$ and $LiNbO_3$ since dispersion equation for Er:$LiNbO_3$ is not available in literature.

In order to compute the modal field of the waveguide, we develop a full vectorial finite-element program based on the Rayleigh-Ritz approach [10], [14]. The program can take into account an arbitrary index distribution. In order to accurately

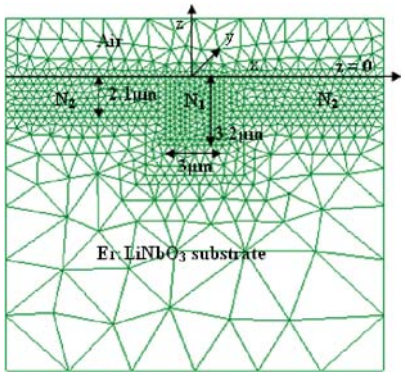

Fig. 4. Waveguide cross section and finite element mesh for the modal analysis of the z-cut y-propagating Er:$LiNbO_3$ waveguide.

discretize the required waveguide geometry through a suitable triangular finite element mesh, we use a commercial computer-aided design tool. Fig. 4 shows the finite element mesh made up of 1410 second-order triangular elements and 2879 nodal points; it is generated in order to discretize the waveguide transverse cross section in the x–z plane. Note that the thickness of the waveguide core (3.2 μm) corresponds to the refractive index variations induced by ion implantation along the waveguide depth.

Using the developed program, the lateral core dimension (3 μm) is optimized in order to ensure single mode operation at both pump (980 nm) and signal (1531 nm) wavelengths. The index profiles N_2 (i.e. for the region under the metallic mask) in Fig. 4 are simply a translation of the N_1 (i.e. for the region under the unmasked surface) profile by the thickness of the metallic mask (1.1 μm) towards the waveguide surface. Considering the anisotropy of the z-cut Er:$LiNbO_3$ crystal, we assume diagonal refractive index matrices for the implanted waveguide where $n_{xx}(z) = n_{yy}(z) = n_o(z)$ (ordinary index) and $n_{zz}(z) = n_e(z)$ (extraordinary index), whereas constant indices are considered for the virgin substrate (i.e. $n_{xx}(z) = n_{yy}(z) = n_o$ and $n_{zz}(z) = n_e$). The fundamental mode intensity profiles computed by our VFEM based program for π-polarization (with major component of electric field polarized parallel to the optical axis (c), i.e. z-axis of the waveguide) at both laser and pump wavelengths are shown in Fig. 5. The program can also take into account multimode operations by considering the fraction of several guided modes that can be excited at both signal and pump wavelengths [10]. However, in this paper, we shall restrict our analysis to single mode operations as it is often preferred while designing integrated waveguide amplifiers and lasers for communication systems.

From the surface plot of the fundamental mode intensity distribution shown in Fig. 5, we observe a clear overlapping of the pump and laser intensity profiles, which indicates the possibility of having efficient laser emission while pumping the waveguide at 980 nm. The major electric field component is aligned parallel to the z axis of the waveguide. Note that this strong confinement at π-polarization (quasi-TM_{00} mode) is achieved mainly due to the extraordinary index raised guiding region between the air and the low index substrate. We also

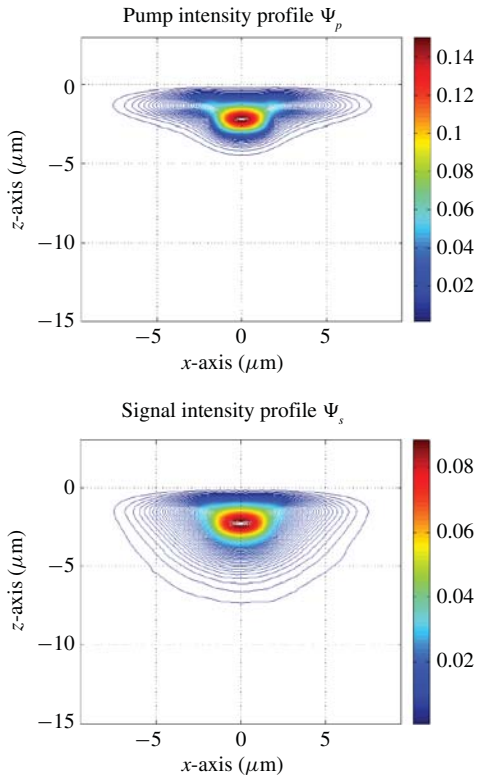

Fig. 5. Fundamental mode intensity profiles (π-polarization) at pump (λ = 980 nm) and laser (λ = 1531 nm) wavelengths, computed by our VFEM code. Corresponding mode effective indices are $n_{eff} = 2.166802$ at the pump wavelength and $n_{eff} = 2.140318$ at the signal wavelength. The density power Ψ_p and Ψ_s are shown in μm^{-2}.

investigate the light confinement for σ-polarization (quasi-TE modes, i.e. $E \perp c$, where c is the optical axis of the crystal). Since ion implantation lowers the ordinary refractive index value, the modes for σ-polarization are usually less confined and show a serious tunnelling effect with significant light leakage into the substrate region, eventually resulting in higher losses [15]. In our simulation we do not find good confinement of quasi-TE modes at longer wavelengths. In fact, from an experimental point of view, these waveguides behave as polarizing filters. Therefore, we perform the analysis for π-polarized light only.

IV. Theoretical Laser Model

In our model, we assume a three level Er^{3+} laser system to be pumped at 980 nm, taking into account the uniform up-conversion process from the meta-stable level $^4I_{13/2}$, and the excited state absorption (ESA) from the pump level $^4I_{11/2}$. The major transitions included in the model are shown in Fig. 6. Note that the upper levels, whose population densities are neglected, are shown in the figure with dotted lines to describe the ESA and upconversion mechanisms only; they are not included in the rate equation. The upper levels are only populated due to ESA and up-conversion described by the transition rate R_{ESA} and up-conversion coefficient C_{up}. A rapid relaxation of ions occurs to its immediate lower levels by non-radiative decay. We expect significant ESA effects due to the relatively long lifetime of the $^4I_{11/2}$ pump level at 980 nm,

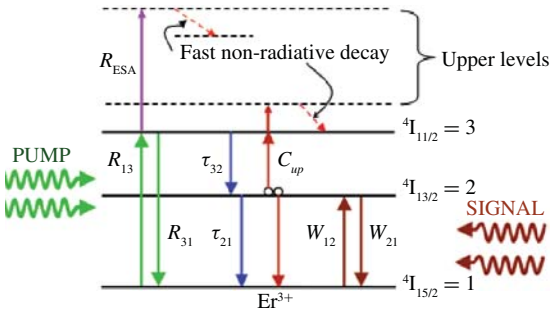

Fig. 6. Three-level Er^{3+} laser system for 980 nm pumping scheme and relative transitions used in our model.

which are confirmed by the following analysis. Due to the co-operative up-conversion process from the meta-stable level, energy transfer occurs between two excited erbium ions in the meta-stable level $^4I_{13/2}$: one is promoted to a higher energy level and then falls down to level $^4I_{11/2}$, while the other returns to ground level with consequent reduction of the population inversion and performance degradation at high Er^{3+} concentration levels.

The population for the three-level system is described by the following rate equations [16]

$$\frac{\partial n_1}{\partial t} = -(W_{12} + R_{13})n_1 + \left(W_{21} + \frac{1}{\tau_{21}}\right)n_2 + R_{31}n_3 + C_{UP}n_2^2 \quad (1)$$

$$\frac{\partial n_2}{\partial t} = W_{12}n_1 - \left(W_{21} + \frac{1}{\tau_{21}}\right)n_2 + \frac{1}{\tau_{32}}n_3 - 2C_{UP}n_2^2 \quad (2)$$

$$\frac{\partial n_3}{\partial t} = R_{13}n_1 - \left(R_{31} + \frac{1}{\tau_{32}}\right)n_3 + C_{UP}n_2^2 \quad (3)$$

where W_{ij} and R_{ij} are the laser and pump induced transition rates respectively absorption ($i < j$) and emission ($i > j$) between the levels i-th and j-th, n_k represents the populations of relevant Er^{3+} energy levels ($k = 1, 2, 3$) and τ_{ij} stands for the lifetime of erbium ions at different levels. The uniform up-conversion process is described by the concentration dependent up-conversion coefficient C_{up}. Using the conservation law, we can write

$$N_{Er} = n_1 + n_2 + n_3 \quad (4)$$

where, N_{Er} is the total erbium concentration in the active medium. The transition rates are described by the following expressions

$$W_{12} = \sum_{i=1}^{M} \frac{\sigma_{12}(\upsilon_i)}{h\upsilon_i}\left[I^+_{ASE}(x,z) + I^-_{ASE}(x,z)\right] \quad (5)$$

$$W_{21} = \sum_{i=1}^{M} \frac{\sigma_{21}(\upsilon_i)}{h\upsilon_i}\left[I^+_{ASE}(x,z) + I^-_{ASE}(x,z)\right] \quad (6)$$

$$R_{13} = \frac{\sigma_{13}(\upsilon_p)I_p(x,z)}{h\upsilon_p} \quad (7)$$

$$R_{31} = \frac{\sigma_{31}(\upsilon_p)I_p(x,z)}{h\upsilon_p} \quad (8)$$

where h is the Plank's constant, M is the number of frequency slots of width $\Delta\upsilon_i$ centred at frequency υ_i and used for the discretization of the amplified spontaneous emission (ASE) spectrum, $I^{\pm}_{ASE}$ and I_p are the ASE (co- and counter-propagating) and pump intensities at frequencies υ_i (laser) and υ_p (pump) respectively. The absorption and emission cross sections are shown as σ_{12} or σ_{21} (for laser light) and σ_{13} or σ_{31} (for pump). Finally, the steady state evolution of pump (P_p) and $ASE \pm (P^{\pm}_{ASE})$ powers along the propagation direction (y) can be described by the following propagation equations

$$\frac{dP_p}{dy} = P_p\int_A \left[\sigma_{31}(\upsilon_p)n_3 - \sigma_{13}(\upsilon_p)n_1 - \sigma_{ESA}(\upsilon_p)n_3\right] \cdot \Psi_p dA - l_p P_p \quad (9)$$

$$\frac{dP^{\pm}_{ASE_i}}{dy} = \pm P^{\pm}_{ASE_i}\int_A \left[\sigma_{21}(\upsilon_i)n_2 - \sigma_{12}(\upsilon_i)n_1\right]\cdot\Psi_S dA \pm mh\upsilon_i\Delta\upsilon_i\int_A \sigma_{21}(\upsilon_i)n_2\Psi_S dA \mp l_S P^{\pm}_{ASE} \quad (10)$$

where ψ_p and ψ_s are the normalized mode intensity profiles (assumed to be invariant along y) at pump and signal wavelengths correspondingly, A is the cross sectional (x–z plane) area of the active region of the waveguide (Er:$LiNbO_3$), l_p and l_s are the background losses at pump and signal wavelengths respectively, σ_{ESA} is the ESA cross section at pump wavelength, and m represents the number of guided modes propagating at the laser wavelength, which is 2 in a single mode guide due to the two fundamental TE and TM modes [17]. In our simulation, m is equal to 1 since we consider only the π-polarized fundamental signal mode to be guided along the propagation direction. The following laser boundary conditions are introduced

$$P^-_{ASE}(L,\upsilon_s) = R_2 P^+_{ASE}(L,\upsilon_s) \quad (11)$$

$$P^+_{ASE}(0,\upsilon_s) = R_1 P^-_{ASE}(0,\upsilon_s) \quad (12)$$

where L is the length of the laser cavity and R_1, R_2 are the input and output reflectivity respectively. The cavity is considered to be nonresonant at the pump (980 nm) wavelength and mono-modal at the lasing wavelength (1531 nm). We assume a dielectric mirror at the input and a Bragg reflector at the output. Note that an equivalent input noise bandwidth $\Delta\upsilon_i$ is included in (10) to start the possible oscillation process. The propagation equations, coupled with the rate equations, are then numerically solved by combining the VFEM program, which computes the normalized intensity profiles ψ_p at the pump and ψ_s at signal wavelength (figure 5), and a Runge-Kutta based iterative procedure which integrates the propagation equations [10].

V. Laser Design

The model described in the previous section is used for the design of a CW laser based on a z-cut ion implanted Er:$LiNbO_3$ embedded waveguide, taking into account the real refractive index variation of our waveguide sample caused by carbon ion implantation. A typical schematic of the z-cut y-propagating Er:$LiNbO_3$ laser cavity is shown in Fig. 7, where we exploit a single pass pumping scheme. The absorption and emission cross sections for the Er:$LiNbO_3$ are taken from [17]. The spectra shown in Fig. 8 are reproduced by numerical fitting with a discretization of 165 (M) frequency

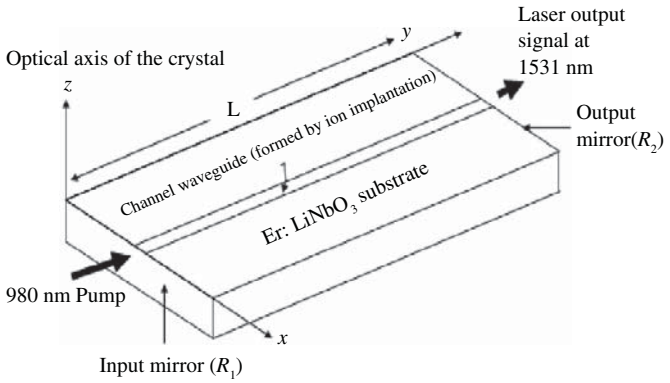

Fig. 7. Schematic of an ion implanted z-cut y-propagating Er:$LiNbO_3$ waveguide laser.

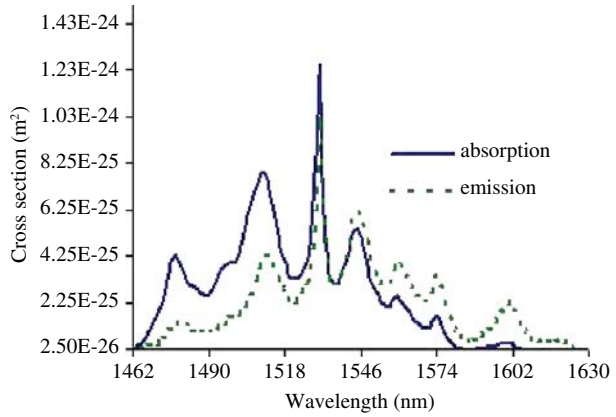

Fig. 8. Absorption (solid line) and emission (dashed line) cross sections for π-polarization of Er:$LiNbO_3$ reproduced from [17] by numerical fitting.

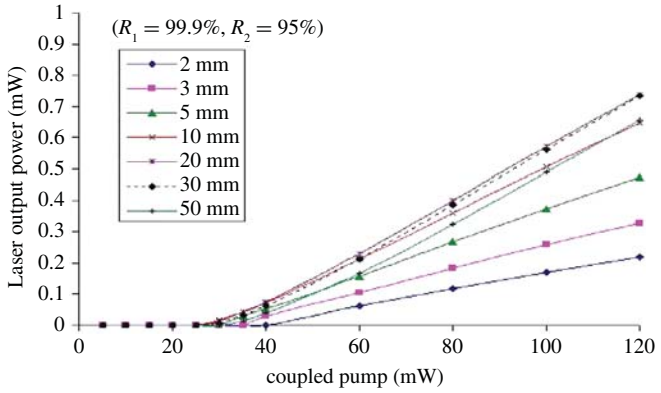

Fig. 9. Computed laser output power as a function of coupled pump power for different laser cavity lengths (L).

slots (from 1462 nm to 1626 nm) and a resolution of 1 nm ($\Delta\upsilon_i$). Note that the use of such spectra is justified by recent studies showing that the fluorescence properties of rare earth ions are not deteriorated in the doped crystal due to ion implantation process [12], [18], [19]. It can be seen that the cross section curves are not as uniform as that of Er^{3+} doped glasses, pointing out that the fabricated waveguide is more appropriate for lasing devices rather than amplifiers for wavelength division multiplexing (WDM) application. The general input parameters used in our model are summarized in Table I.

TABLE I
LASER INPUT PARAMETERS USED IN OUR MODEL

Parameters	Values	Ref.
Absorption cross section at 1531 nm, σ_{12}	1.25×10^{-24}m^2	[17]
Stimulated Emission cross section at 1531nm, σ_{21}	1.03×10^{-24}m^2	[17]
Life time $^4I_{13/2} - {}^4I_{15/2}$, τ_{21}	4.3 ms	[17]
Life time $^4I_{11/2} - {}^4I_{13/2}$, τ_{32}	200 μs	[20]
ESA cross section at 980 nm, σ_{ESA}	0 m^2	
Stimulated Emission cross section at 980 nm, σ_{31}	0 m^2	[20]
Total Erbium concentration, N_{Er}	1.0×10^{26}m^{-3}	[20]
Up-conversion coefficient at N_{Er}, C_{UP}	1.0×10^{-24}m^{3}s^{-1}	[20]
Background loss at signal wavelengths, l_s	20 dB/m	[20]
Background loss at pump wavelengths, l_p	30 dB/m	[20]
Absorption cross section at 980 nm, σ_{13}	0.20×10^{-24}m^2	[21]
Signal effective index, n_s^{eff} (π-polarization)	2.140318	
Pump effective index, n_p^{eff} (π-polarization)	2.166802	
Input mirror reflectivity, R_1	99.90%	
Output mirror reflectivity, R_2	95%	

TABLE II
ESA PARAMETER [20]

ESA cross section, σ_{ESA}	values
ESA0	0 m^2
ESA1	1×10^{-26} m^2
ESA2	2×10^{-25} m^2
ESA3	1×10^{-24} m^2

VI. RESULTS AND DISCUSSIONS

With the general input parameters shown in Table I, we study the characteristics of laser output and its dependence on various input waveguide parameters. Note that, as a preliminary case, we perform our simulations without considering excited state absorption (ESA), i.e. assigning $\sigma_{ESA} = 0$ in (9), from the pump level.

We later introduce ESA in order to quantify its impact on the laser performance. Optimum erbium concentration is not investigated mainly due to the unavailability of concentration dependent up-conversion coefficient (C_{UP}) values for Er:$LiNbO_3$. Fig. 9 shows the predicted laser output for different cavity lengths. Lasing thresholds are found to be affected by the cavity lengths. An optimum waveguide length (see Fig. 10) is identified between 15 mm and 20 mm with a threshold coupled pump power of 25 mW.

The figure 11 reports the effects of ESA on the laser performance with the cavity length of 5 cm. The ESA cross section values are taken from [20] and are listed in Table II.

The laser output power is found to be drastically reduced when the ESA cross section values increase. However, the laser threshold remains unaffected. The ESA values also depend on the pump level lifetime which is fabrication process dependent. While measuring these values, care must be taken in order to predict a more realistic performance from the fabricated device.

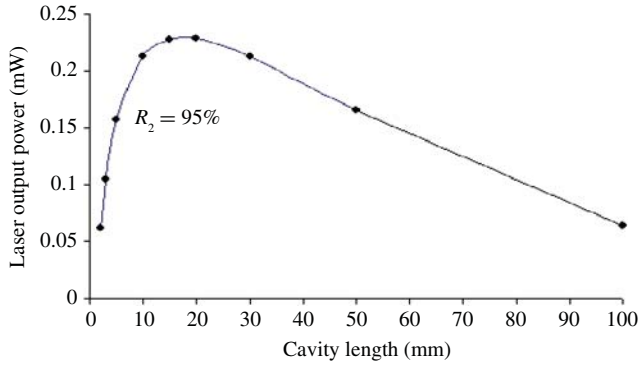

Fig. 10. Laser output computed at 60 mW coupled pump power with different cavity lengths.

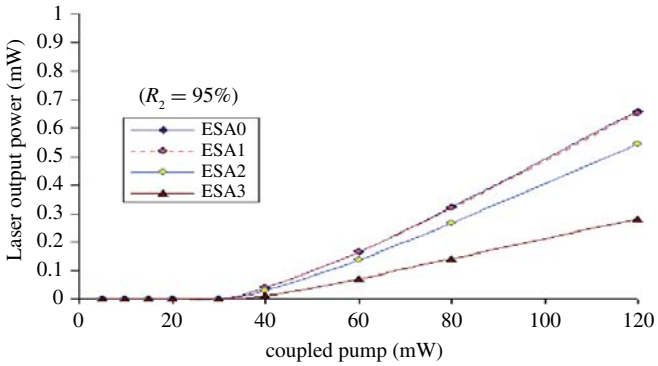

Fig. 11. Computed laser output as a function of coupled pump power for a 5 cm long cavity with varying ESA cross sections.

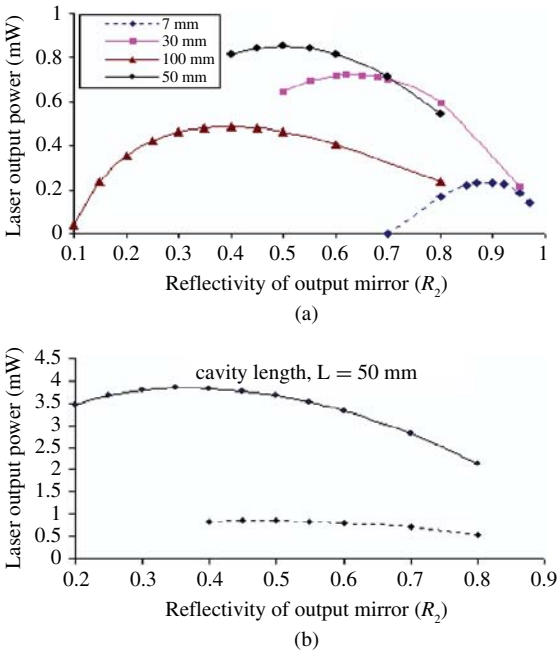

Fig. 12. (a) Computed laser output at different cavity lengths as a function of the reflectivity of the output mirror (R_2) for 60 mW pump, and (b) laser output for a 5 cm long cavity with 60 mW (dashed line) and 120 mW (solid line) coupled pump power.

Finally, we investigate the dependence of laser performances on the reflectivity of the output mirror (R_2). Fig. 12a shows the laser output power at 1531 nm for different reflectivity

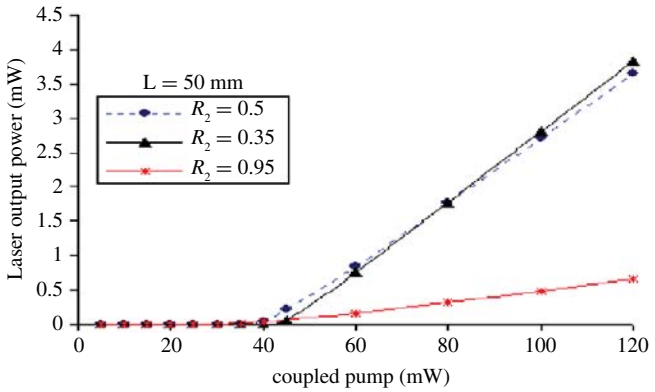

Fig. 13. Computed laser output for a 5 cm long cavity as a function of coupled pump power and different reflectivity (R_2).

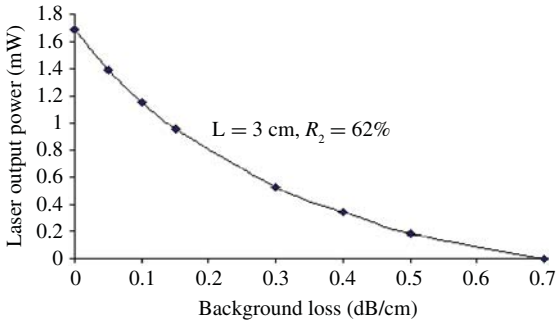

Fig. 14. Computed laser output as a function of background losses at 60 mW coupled pump power and a cavity length of 3 cm. Background losses are considered equal at both pump (980 nm) and laser (1531 nm) wavelengths.

(R_2) values, fixing the input coupled pump power at 60 mW. Note that, for each cavity length, there is an optimum value of R_2 for which the laser output power is the highest. It is also observed that this optimum reflectivity depends on the coupled pump power. For example, a 5-cm long cavity with 60 mW and 120 mW (Fig. 12b) pumped powers gives respectively 0.5 and 0.35 as optimum values for R_2. Computed laser output powers at both R_2 values (0.5 and 0.35) are plotted in Fig. 13, where a higher threshold is noted for the output reflectivity of 0.35.

In order to optimize the laser cavity, both the waveguide length and the output reflectivity should be adjusted simultaneously. Laser outputs for different background losses are plotted in Fig. 14, considering a 3-cm laser cavity with the optimum output reflectivity ($R_2 = 0.62$). The background losses are assumed equal at both pump and laser wavelengths. As expected, we see a clear degradation of the laser output power with higher background losses. It is also noted that the waveguide laser does not reach the lasing threshold for losses greater than 0.7 dB/cm. Therefore, it is important to minimize such losses during the fabrication process.

VII. Conclusion

We have theoretically demonstrated an efficient lasing performance of a z-cut y-propagating Er:$LiNbO_3$ waveguide produced through high energy ion implantation.

Ion implantation has been performed on a z-cut Er:$LiNbO_3$ substrate with carbon ions (C^{3+}), forming embedded channel waveguides suitable for the third telecommunication window. We have shown by VFEM based modal analysis a good confinement of π-polarized light. Through simulations, we have been able to identify an optimized waveguide geometry (3 μm $\times$ 3.2 μm core dimension) for the Er:$LiNbO_3$ waveguide laser, which allows single mode operation at both pump (980 nm) and lasing wavelengths (1531 nm). However, we have not observed good power confinement for σ-polarized light.

Having considered the measured refractive index variation of the implanted waveguide sample and other realistic spectroscopic data, we have simulated the steady state operation of a waveguide laser optically pumped at 980 nm. We assumed a three energy level system for our model, taking into account excited state absorption (ESA) and uniform up- conversion. We have investigated laser performance and analyzed its characteristic as a function of various waveguide parameters. Efficient lasing was observed for a 2-cm cavity with a low threshold coupled pump power (25 mW) having the output mirror reflectivity of 95%. About 4 mW of maximum output power has been predicted from a 5-cm cavity for a threshold pump power of 45 mW.

In addition, we have shown that the laser threshold and output power are greatly affected by various parameters like cavity length, output reflectivity, ESA and background losses. In particular, background losses were found to be quite detrimental. Our model also indicated that, for a proper design of the laser cavity, output reflectivity and cavity length should be adjusted simultaneously. The spectroscopic properties should be investigated in further detail in order to predict precise and more realistic lasing performance from our waveguide sample; this topic is now under further investigation. However, the results that we have presented in this paper provide us many important indications on the optimization of a z-cut y propagating Er:$LiNbO_3$ waveguide lasers fabricated through high energy ion implantation.

REFERENCES

[1] F. Caccavale, F. Segato, and I. Mansour, "A numerical study of erbium doped active $LiNbO_3$ waveguides by the beam propagation method," *J. Lightw. Technol.*, vol. 15, no. 12, pp. 2294–2300, Dec. 1997.

[2] I. Baumann, S. Bosso, R. Brinkmann, R. Corsini, M. Dinand, A. Greiner, K. Schafer, J. Sochtig, W. Sohler, H. Suche, and R. Wessel, "Er-doped integrated optical devices in $LiNbO_3$," *IEEE J. Sel. Topics Quantum Electron.*, vol. 2, no. 2, pp. 355–366, Jun. 1996.

[3] S.-L. Li, K.-M. Wang, F. Chen, X.-L. Wang, G. Fu, D.-Y. Shen, H.-J. Ma, and R. Nie, "Monomode optical waveguide excited at 1540 nm in $LiNbO_3$ formed by MeV carbon ion implantation at low doses," *Opt. Exp.*, vol. 12, no. 5, pp. 747–752, Mar. 2004.

[4] F. Chen, X.-L. Wang, and K.-M. Wang, "Development of ion-implanted optical waveguides in optical materials: A review," *Opt. Mater.*, vol. 29, no. 11, pp. 1523–1542, Jul. 2007.

[5] A. Guarino, G. Poberaj, D. Rezzonico, R. Degl'Innocenti, and P. Gunter, "Electro-optically tunable microring resonators in lithium niobate," *Nature Photon.*, vol. 1, pp. 407–410, Jul. 2007.

[6] A. Majkic, G. Poberaj, and P. Gunter, "Optical microring resonators in fluorine-implanted lithium niobate for electrooptical switching and filtering," *IEEE Photon. Technol. Lett.*, vol. 21, no. 10, pp. 639–641, May 2009.

[7] M. Koechlin, F. Sulser, Z. Sitar, G. Poberaj, and P. Gunter, "Free-standing lithium niobate microring resonators for hybrid integrated optics," *IEEE Photon. Technol. Lett.*, vol. 22, no. 4, pp. 251–253, Feb. 2010.

[8] F. Sulser, G. Poberaj, M. Koechlin, and P. Gunter, "Photonic crystal structures in ion-sliced lithium niobate thin films," *Opt. Exp.*, vol. 17, no. 22, pp. 20291–20300, Oct. 2009.

[9] M. Bianconi, G. G. Bentini, M. Chiarini, P. De Nicola, G. B. Montanari, A. Nubile, and S. Sugliani, "Defect engineering and micromachining of lithium niobate by ion implantation," *Nucl. Instrum. Methods Phys. Res. Sect. B: Beam Interact. Mater. At.*, vol. 267, no. 17, pp. 2839–2845, Sep. 2009.

[10] F. Di Pasquale and M. Zoboli, "Analysis of erbium-doped waveguide amplifiers by a full-vectorial finite-element method," *J. Lightw. Technol.*, vol. 11, no. 10, pp. 1565–1574, Oct. 1993.

[11] S. Sugliani, M. Bianconi, G. G. Bentini, M. Chiarini, P. De Nicola, G. B. Montanari, A. Menin, A. Malacarne, and L. Potì, "Refractive index tailoring in congruent lithium niobate by ion implantation," *Nucl. Instrum. Methods Phys. Res. B: Beam Interact. Mater. At.*, vol. 268, no. 19, pp. 2911–2914, Oct. 2010.

[12] G. G. Bentini, M. Chiarini, M. Bianconi, F. Bergamini, D. Castaldini, G. B. Montanari, A. Bogoni, L. Potì, S. Sugliani, A. Nubile, P. De Nicola, L. Gallerani, G. Pennestrì, and S. Petrini, "Waveguide formation by ion implantation in Er doped optical materials," *Nucl. Instrum. Methods Phys. Res. B: Beam Interact. Mater. At.*, vol. 266, nos. 12–13, pp. 3120–3124, Jun. 2008.

[13] S. D. Smith, H. D. Riccius, and R. P. Edwin, "Refractive indices of lithium niobate," *Opt. Commun.*, vol. 17, no. 3, pp. 332–335, Jun. 1976.

[14] J. Jin, *The Finite Element Method in Electro-Magnetics*, 2nd ed. New York: Wiley, 2002.

[15] F. Chen, X.-L. Wang, F. Lu, and K.-M. Wang, "Property investigation of C^+-ion-implanted $LiNbO_3$ planar optical waveguides," *J. Appl. Phys.*, vol. 98, no. 4, pp. 044507-1–044507-5, Aug. 2005.

[16] P. Pintus, S. Faralli, V. Toccafondo, F. Di Pasquale1, A. D'Errico, and F. Testa, "Design of optically pumped Er^{3+} doped silicon-on-insulator slot waveguide lasers," in *Proc. Conf. IEEE LEOS Ann. Meeting*, Antalya, Turkey, Oct. 2009, pp. 301–302.

[17] C.-H. Huang, L. M. Caughan, and D. M. Gill, "Evaluation of absorption and emission cross sections of Er-doped $LiNbO_3$ for application to integrated optic amplifiers," *J. Lightw. Technol.*, vol. 12, no. 5, pp. 803–809, May 1994.

[18] F. Chen, Y. Tan, and A. Rodenas, "Ion implanted optical channel waveguides in Er^{3+}/MgO co-doped near stoichiometric $LiNbO_3$: A new candidate for active integrated photonic devices operating at 1.5 μm," *Opt. Exp.*, vol. 16, no. 20, pp. 16209–16214, Sep. 2008.

[19] N.-N. Dong, F. Chen, and D. Jaque, "Carbon ion implanted Nd:MgO:$LiNbO_3$ optical channel waveguides: An intermediate step between light and heavy ion implanted waveguides," *Opt. Exp.*, vol. 18, no. 6, pp. 5951–5956, Mar. 2010.

[20] D. L. Veasey, J. M. Gary, J. Amin, and J. A. Aust, "Time-dependent modeling of erbium-doped waveguide lasers in lithium niobate pumped at 980 and 1480 nm," *IEEE J. Quantum Electron.*, vol. 33, no. 10, pp. 1647–1662, Oct. 1997.

[21] C.-H. Huang and L. M. Caughan, "980-nm-pumped Er-doped $LiNbO_3$ waveguide amplifiers: A comparison with 1484 nm pumping," *IEEE J. Sel. Topics Quantum Electron.*, vol. 2, no. 2, pp. 367–372, Jun. 1996.

Sohel Mahmud Sher received the B.Sc. degree in electronics and communications engineering from Khulna University, Khulna, Bangladesh, in 2001, and the Masters degree in telecommunications engineering from the Asian Institute of Technology, Pathum Thani, Thailand, in 2006. He has been pursuing the Ph.D. degree in information and communication engineering from the Scuola Superiore Sant'Anna, Pisa, Italy, since January 2008.

He is working in the research areas of optical amplifiers and lasers. His current research interests include lithium-niobate-based waveguide lasers and microring resonators for telecommunication applications.

Paolo Pintus (S'10) was born in Cagliari, Italy, in 1983. He received the Bachelors degree with honors in electronic engineering and the Masters degree with honors from the University of the Studies of Cagliari, Cagliari, in 2005 and 2007, respectively. He is currently pursuing the Ph.D. degree at the Scuola Superiore di Studi Universitari e Perfezionamento Sant'Anna, Pisa, Italy.

He was a Visiting Student (Leonardo da Vinci program) at the Crisanti Laboratory, Department of Biological Sciences, Imperial College London, London, U.K., in 2007, where he was involved in signal processing and pattern recognition on malaria vaccine detection. His current research interests include silicon photonics and integrated optics.

Fabrizio Di Pasquale (M'04) was born in Italy in 1963. He received the degree in electronic engineering from the University of Bologna, Bologna, Italy, in 1989, and the Ph.D. degree in information technology from the University of Parma, Parma, Italy, in 1993.

He was with the Department of Electrical and Electronic Engineering, University College London, London, U.K., as a Research Fellow, from 1993 to 1998, working on optical amplifiers, wavelength-division multiplexing (WDM) optical communication systems, and liquid crystal displays. After 2 years with Pirelli Cavi e Sistemi, Milan, Italy, and 2 years with Cisco Photonics, Monza, Italy, he is currently an Associate Professor in telecommunications at the Scuola Superiore Sant'Anna, Pisa, Italy. He has filed 15 international patents and is the author or co-author of over 120 papers in scientific journals and conference proceedings in the areas of optical amplifiers, optical communications systems, liquid crystal displays, and distributed optical fiber sensors. His current research interests include optical amplifiers, WDM transmission systems and networks, and optical fiber sensors.

Prof. Di Pasquale is on the Board of Reviewers of IEEE PHOTONICS TECHNOLOGY LETTERS, IEEE/OSA, *Journal of Lightwave Technology, Optics Communications, Optics Express*, and *Optics Letters.*

Marco Bianconi received the Laurea degree in physics from the University of Bologna, Bologna, Italy, in 1984.

He joined the permanent staff of the Institute for Microelectronics and Microsystems of the Italian National Research Council, Bologna, in 1988. He is currently the Head of the Ion Beam Department and the Director of the Regional Network Laboratory Laboratorio di Micro e Submicro Tecnologie Abilitanti dell'Emilia-Romagna, Bologna. His current research interests include high-energy ion implantation of semiconductors and insulators for applications in micro- and opto-electronics, photonics, microsystems, top-down approach to nanotechnologies, study of the ion-matter interaction, and development of analytical techniques based on ion beams.

Giovanni Battista Montanari received the B.S., M.S., and Ph.D. degrees in electrical engineering from the University of Bologna, Bologna, Italy, in 2003, 2005, and 2010, respectively.

He is currently a Research Assistant at the Institute for Microelectronics and Microsystems of National Research Council, Bologna, within the Regional Network Laboratory Regional Network Laboratory Laboratorio di Micro e Submicro Tecnologie Abilitanti dell'Emilia-Romagna, Bologna. In 2009, he was a Visiting Researcher at Stanford University, Stanford, CA, working with Prof. K. Saraswat's group on spintronic devices. His current research interests include manufacturing, design, and characterization of integrated optic devices based on ion-implanted lithium niobate, silicon photonics, and spintronics.

Pietro De Nicola received the Masters degree with honors in physics from the University of Bologna, Bologna, Italy, in 2006, with a thesis on vibrating microreed gas sensing.

He has been working as a Research Assistant in the Institute for Microelectronics and Microsystems of the National Research Council, Bologna, since 2006, within the Regional Network Laboratory Regional Network Laboratory Laboratorio di Micro e Submicro Tecnologie Abilitanti dell'Emilia-Romagna, Bologna. His current research interests include effects of high-energy ion implantation on chemical, optical, and electrooptical properties of lithium niobate, lithium niobate-based optoelectronic devices, and electronic emission from ferroelectrics.

Simone Sugliani received the Masters degree in materials engineering from the Politecnico di Milano, Milan, Italy, in 1999, and the second-level Masters degree in optical systems and networks in 2001.

He was with the Consorzio Nazionale Interuniversitario per le Telecomunicazioni at the Photonic Networks National Laboratory, Pisa, Italy, as a Research Assistant. He has been working as a Research Assistant at the Institute for Microelectronics and Microsystems of the National Research Council, Bologna, Italy, since 2005, within the Regional Network Laboratory Regional Network Laboratory Laboratorio di Micro e Submicro Tecnologie Abilitanti dell'Emilia-Romagna, Bologna. His current research interests include manufacturing, design and characterization of optoelectronic and integrated optics devices based on ion-implanted lithium niobate, and optical amplification in wavelength division multiplexing systems.

Giancarlo Prati (M'80–SM'02–F'04) was born in Rome, Italy, in 1946. He received the Graduate degree (*cum laude*) in electronic engineering from Pisa University, Pisa, Italy, in 1972.

He was a Visiting Scientist at the University of Southern California, Los Angeles, where he worked in optical communications, from 1978 to 1979. He was a Visiting Associate Professor at the University of Massachusetts, Amherst, in 1982. He was a Researcher with the Center for Radio Transmission, Pisa, until 1986. He was a Professor of telecommunications, Genoa University, Genoa, Italy, in 1986. He joined Parma University, Parma, Italy, in 1988, where he was the Dean of the Engineering Faculty from 1992 to 1998. He was the Director of the Consorzio Nazionale Interuniversitario per le Telecomunicazioni (CNIT), Pisa. He moved to the Scuola Superiore Sant'Anna, Center of Excellence for Information, Communication, and Perception Engineering (CEIICP), Pisa, in 2000, to create a new research center on photonic networks. He pioneered the area of free-space optical communications for deep-space applications in the late 1970s and early 1980s at the University of Southern California. Since then, he has been promoted and managed several national/international projects on optical communications. He has authored or co-authored more than 70 research papers and has been awarded several patents.

Prof. Prati was a co-recipient of the "W. Bennett" Prize Paper Award in 1987 for his work on blind "stop-and go" equalization of communication channels. He is currently General Co-Chairman of the European Conference on Optical Communication in 2010, member of the Information and Communication Technology Panel of the European Research Council, Director of CEIICP and the President of CNIT. He was a member of the Scientific Committee of the Italian Space Agency from 1997 to 1999.